An Observational Study of Derecho-Producing Convective Systems

MICHAEL C. CONIGLIO

Cooperative Institute for Mesoscale Meteorological Studies/School of Meteorology, University of Oklahoma, and NOAA/OAR/National Severe Storms Laboratory, Norman, Oklahoma

DAVID J. STENSRUD

NOAA/OAR/National Severe Storms Laboratory, Norman, Oklahoma

MICHAEL B. RICHMAN

School of Meteorology, University of Oklahoma, Norman, Oklahoma

(Manuscript received 21 January 2003, in final form 8 September 2003)

ABSTRACT

This study identifies the common large-scale environments associated with the development of derecho-producing convective systems (DCSs) from a large number of events. Patterns are identified using statistical clustering of the 500-mb geopotential heights as guidance. The majority of the events (72%) fall into three main patterns that include a well-defined upstream trough (40%), a ridge (20%), and a zonal, low-amplitude flow (12%), which is identified as an additional warm-season pattern. Consequently, the environmental large-scale patterns idealized in past studies only depict a portion of the full spectrum of the possibilities associated with the development of DCSs.

In addition, statistics of derecho proximity-sounding parameters are presented relative to the derecho life cycle as well as relative to the forcing for upward motion. It is found that the environments ahead of maturing derechos tend to moisten at low levels while remaining relatively dry aloft. In addition, derechos tend to decay as they move into environments with less instability and smaller deep-layer shear. Low-level shear (instability) is found to be significantly higher (lower) for the more strongly forced events, while the low-level storm-relative inflow tends to be much deeper for the more weakly forced events. Furthermore, discrepancies are found in both low-level and deep-tropospheric shear parameters between observations and the shear profiles considered favorable for strong, long-lived convective systems in idealized simulations. This study highlights the need to examine DCS simulations within more realistic environments to help reconcile these disparities in observations and idealized models and to provide improved information to forecasters.

1. Introduction

A derecho-producing convective system (DCS) is a type of mesoscale convective system (MCS; Zipser 1982) that produces large swaths of severe ''straight-line'' winds at the earth's surface. Straight-line winds attributed to convection are typically grouped into those generated by ''mesohighs'' (Johnson and Hamilton 1988), ''gust fronts'' (Goff 1976; Wakimoto 1982), or ''downbursts'' (Fujita and Wakimoto 1981). Much of the damage owing to nontornadic convective winds has been attributed to derechos (Wakimoto 2001). Although derechos appear to occur most frequently during the summer months across the midwestern United States, they have been observed during all months of the year and in most locales east of the Rocky Mountains (Johns and Hirt 1987; Bentley and Mote 1998).

Johns and Hirt (1987; JH87 hereafter) define a derecho[1] as a family of downburst clusters (Fujita and Wakimoto 1981) across an area whose major axis is at least 400 km (see JH87 for a more complete definition). Many types of extratropical MCSs (Maddox 1980; Zipser 1982; Parker and Johnson 2000) can produce derechos. Through a study of 70 warm-season (May–August) cases, JH87 show that the downbursts and strong surface winds are usually associated with ''line echo wave patterns'' (Nolan 1959) and/or ''bow echoes'' (Fujita 1978) in the leading convection. Bow echoes are often observed on a variety of length scales within a

Corresponding author address: Michael C. Coniglio, National Severe Storms Laboratory, 1313 Halley Circle, Norman, OK 73069.
E-mail: Michael.coniglio.@noaa.gov

[1] The term derecho (pronounced day-ray'-cho) was originally defined by Hinrichs (1888) with the intent of distinguishing wind damage produced by ordinary thunderstorm winds from those produced by tornadoes.

DCS (10–300 km) and can be present simultaneously during a single event (JH87; Johns and Doswell 1992; Przybylinski 1995; Weisman 2001). MCSs that contain a small number (one–three) of bow echoes oriented at a large angle to the mean wind direction produce *progressive* derechos, as defined by JH87. More elongated squall lines, sometimes with several individual bow-shaped convective elements that move rapidly along the line generally in the direction of the mean wind, produce *serial* derechos (JH87). Additionally, smaller-scale cyclonic vorticies are often embedded within the main system that may not be associated with identifiable bow-echo circulations. In some cases, these vorticies are directly associated with the most severe wind damage (Schmidt and Cotton 1989; Spoden et al. 1998; Funk et al. 1999; Martinelli et al. 2000; Miller and Johns 2000).

Much of our current knowledge on DCS environments stems from the study of JH87, whose work was restricted to warm-season (and mostly progressive) derechos. West to northwesterly midlevel flow usually overlays a low-level quasi-stationary thermal boundary that is either tied to synoptic flows or to cold outflows from prior convection. The DCSs that occur with relatively weak short-wave troughs generally move at a small angle to this boundary from the cold side to the warm side. The strong trough cases tend to initiate north of a quasi-stationary boundary then develop southward along or just ahead of a traveling cold front. In either case, significant low-level warm advection is usually present near the initiation of convection. Large amounts of conditional and convective instability, related to abnormally moist low levels and relatively dry midlevels, are also found along the derecho track.

Depictions of the large-scale flow patterns associated with DCSs are mostly limited to the severe, long-track variety [Johns et al. (1990) examine 14 such cases]. Upon a synthesis with the results of JH87, this depiction is idealized into a ''warm season'' progressive pattern by Johns (1993) (Fig. 1a). Johns (1993) also idealizes a ''dynamic'' pattern that is thought to occur primarily in association with serial derechos (Fig. 1b). In general, the dynamic pattern consists of a strong, migrating low pressure system and is similar to the more ''classic'' pattern associated with general severe weather outbreaks, in which tornadoes and severe wind outbreaks often occur simultaneously (JH87; Johns and Doswell 1992).

Evans and Doswell (2001) extend the work on derecho environments by examining proximity soundings from 67 DCSs from all times of the year. This work illustrates that derechos occur under a wide range of environmental low-level shear and instability conditions. In addition, they suggest that the strength of the mean flow, and its effect of the motion of MCSs, enhance the potential for sustained severe wind gusts. They also recognize many cases that display features of both the warm-season and dynamic patterns, which suggests that derechos could be classified into additional patterns based on characteristics of these ''hybrids.''

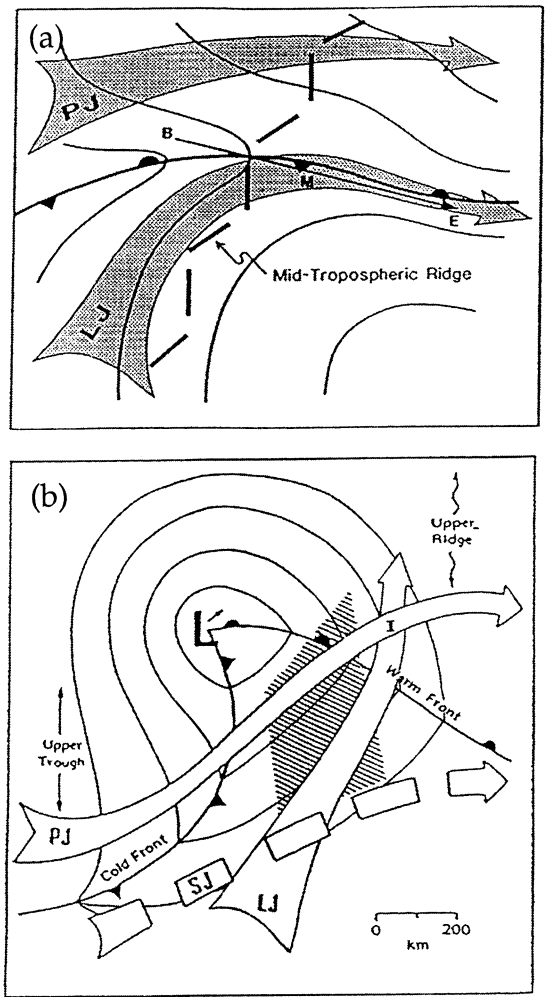

FIG. 1. (a) Idealized sketch of a midlatitude warm-season synoptic-scale pattern favorable for the development of especially severe and long-lived progressive derechos. The line B–M–E represents the track of the derecho. (b) As in (a) except for situations favorable for the development of squall lines with extensive bow-echo-induced damaging winds (serial derechos). The thin lines denote sea level isobars in the vicinity of a quasi-stationary frontal boundary. Broad arrows represent the low-level jet stream (LJ), the polar jet (PJ), and the subtropical jet (SJ) (after Johns 1993).

While the above-mentioned studies reveal many aspects of DCS environments, there has yet to be a comprehensive study documenting the spectrum of large-scale environmental flow patterns associated with DCSs. Therefore, the first goal of this study is to examine this spectrum and to identify, if any, the preferred large-scale patterns from a large dataset of DCS events from all times of the year. Emphasis is placed on more clearly defining and expanding upon the dynamic and warm-season patterns identified in the past literature, primarily for the benefit of those who may use pattern recognition as a part of the forecasting process.

The second goal of this study is to examine DCS environments with the use of proximity soundings for the benefit of ingredients-based forecasting techniques. Section 2 describes the derecho dataset. Section 3 outlines the method used to examine the environmental flow patterns and presents the results. In section 4, the selection of proximity soundings is given and an analysis of the convective available potential energy (CAPE), vertical shear, and moisture profiles is presented. A comparison of these results to past idealized numerical simulations is presented at the end of section 4. The results are summarized in section 5.

2. Derecho dataset

Storm Data, provided by the National Climatic Data Center (NCDC), and the convective wind database complied by the Storm Prediction Center (SPC) are examined for the years of 1980–2001 to identify derecho events. A convectively induced windstorm is considered a derecho if 1) successive severe wind gust ($\geq$26 m s^{-1}) or wind damage reports exhibit a major axis $\geq$400 km in length, 2) the wind reports show a near-continuous progression in a single or series of swaths with no more than 2.5 h or 200 km between successive concentrations of wind reports, and 3) the parent convection is organized into an extratropical system of convective cells and exhibits a distinct linear or bowed radar reflectivity structure.

Like Bentley and Mote (1998), this study does not require the occurrence of at least three reports of wind gusts $\geq$33 m s^{-1} (or wind damage reports rated F1 or greater on the Fujita scale) along the derecho path, as used in JH87. Therefore, this study includes systems that are somewhat more benign than those defined as derechos by JH87. Bentley and Mote (1998) removed this restriction, in part, because of the potential to unnecessarily overlook long-lived severe-wind-producing MCSs (Bentley and Mote 2000). Furthermore, JH87 only consider wind reports during the bow-echo stages of the DCS. In this study, wind reports that occur during the developing or decaying stages of the DCSs are considered part of the derecho paths so that bow echoes and squall lines with shorter lifetimes than those considered in JH87 are included.

Unlike Bentley and Mote (1998), this study retains the requirement from JH87 to examine radar reflectivity structures. This helps to preserve the original intent of JH87 to discriminate windstorms produced by an organized MCS from those produced by more isolated cells (Johns and Evans 2000). The available Weather Surveillance Radar-1988 Doppler (WSR-88D) level II reflectivity data, the WSR-88D mosaic reflectivity images at 2- or 4-km resolution (obtained from SPC and NCDC), or the archived hourly radar summary charts produced by the National Centers for Environmental Prediction (NCEP) are used to examine this criterion.

The time and location of the first severe wind report associated with the convection that becomes the DCS defines the origin of each event. Similarly, the time and location of the last severe wind report or wind damage report associated with the main wind damage path defines the termination of each event. The derecho major axis is obtained by connecting the position of the first and last wind reports through the center of the swath of wind reports. For the cases that have multiple swaths produced by distinct features along the main squall line or MCS (mostly serial derechos), the longest path defines the major axis of the derecho. In most cases, the longest swath is the only swath that satisfies the major axis length criteria given above.

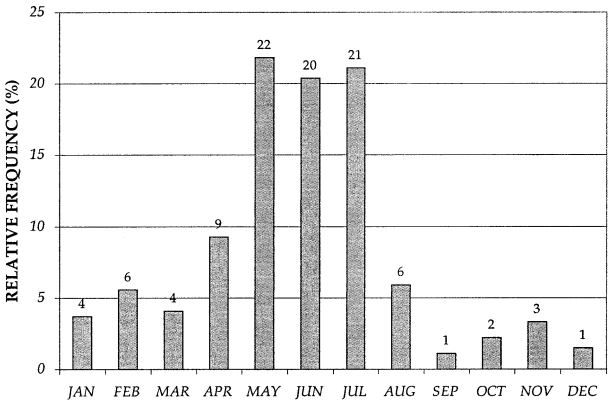

FIG. 2. The relative frequency distribution of the month of occurrence for the 270 derecho events.

The above procedure identifies 270 derecho events. The monthly frequency distribution confirms that derechos occur year-round, but are primarily a warm-season phenomenon (70% of the cases occur in the months of May–August; Fig. 2). The geographical distribution for all months of the year includes two activity corridors that are separately identified by JH87 and Bentley and Mote (1998). These corridors stretch from the upper Midwest to the Ohio valley and from the southern Great Plains to the lower Mississippi valley[2] (Fig. 3a). Two maximum frequency axes also exist for the May–June derecho distribution across the southern plains and across the Midwest (Fig. 3b). The primary axis shifts to the northern plains and the upper Midwest in July and August (Fig. 3c). The distribution for the remaining months (September–April) shows a shift of the primary axis to the south and east across the Gulf coast states (Fig. 3d) and a secondary axis from the western Ohio valley through eastern Pennsylvania (Fig. 3d).

[2] This distribution should not be interpreted as a formal climatology because of the limitations of using *Storm Data* (Johns and Evans 2000) and the difficulty in identifying events near the U.S. border or near ''peninsular'' areas (New England and Florida). Instead, the primary purpose of Figs. 2 and 3 is to show that this dataset represents derecho events from all months of the year and most locales east of the Rocky Mountains.

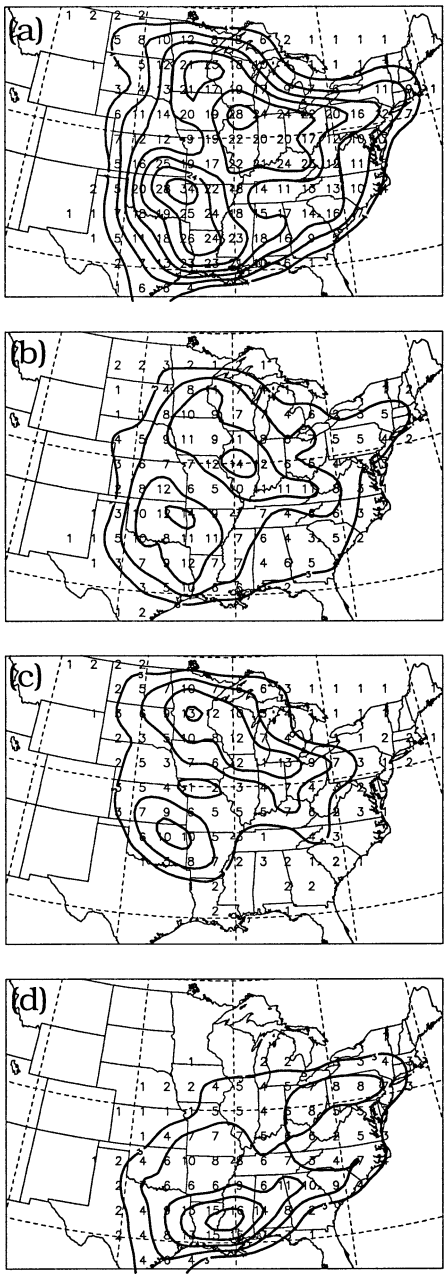

FIG. 3. The total number of derechos in 200 km × 200 km squares for (a) all 270 events, (b) the 114 events during the months of May and Jun, (c) the 73 events during the months of Jul and Aug, and (d) the 83 events during the months of Sep–Apr. Contours are drawn every four events in (a) and every three events in (b)–(d).

3. Large-scale analyses

The goal of identifying typical large-scale flow patterns will be met through the examination of constant pressure analyses that represent the environment during the development of DCSs. This study uses the four times daily analyses (valid at 0000, 0600, 1200, and 1800 UTC) from the NCEP–National Center for Atmospheric Research (NCAR) reanalysis dataset (Kistler et al. 2001). The time of the analysis that is closest to the time of the first wind report is used to represent each case.

Since there is a wide range of durations observed among the events (5–30 h), the environments relative to the life cycle of each event are preserved by defining a normalized observation time, t (if the derecho begins at 0600 UTC and terminates at 1800 UTC, then $t = 0.5$ for the 1200 UTC analysis). The value of t must be estimated for the cases in which the derecho appears to begin (or end) over Canada or over oceanic waters. The dataset is further restricted to include only those cases with $|t| \leq 0.25$. This restriction removes some of the shorter-lived events from the dataset but ensures that environments associated with the initiation and early mature stages of the DCSs are examined. This procedure identifies 225 cases for further analysis.

a. Analysis method

The first goal of this study is to determine if there are preferred large-scale flow patterns associated with the development of DCSs and, if so, the structure of the patterns. In this study, the patterns are first defined by the subjective recognition of the primary synoptic-scale feature that influences each DCS. To supplement the subjective approach, a method based on cluster analysis to the 500-mb geopotential height field (ϕ) is used as guidance. The basic benefit of using a semiobjective technique, such as cluster analysis, is to provide an element of objectivity to determining a meaningful stratification of the data that might otherwise be overlooked in an entirely subjective technique, especially when dealing with a large dataset (Wilks 1995).

In this application, gridpoint values of 500-mb geopotential heights (ϕ) from the representative analysis are interpolated to a Cartesian grid with its origin located at the intersection between the DCS leading edge (or initial convective cluster) and the derecho major axis. Each grid has 27 points in the east–west direction and 25 points in the north–south direction (675 total) spaced 100 km apart. An $n \times p$ data matrix, $\mathbf{X}$, is formed with the 225 cases as the n columns and the 675 gridpoint values of ϕ as the p rows.

Past DCS literature emphasizes the subjective recognition of flow patterns in terms of the shape and orientation of the geopotential heights (JH87; Bentley et al. 2000; Evans and Doswell 2001). A reasonable choice to quantitatively relate the 225 cases in this manner is the Pearson correlation coefficient (Gong and Richman 1995). Application of this measure to $\mathbf{X}$ results in an $n \times n$ symmetric matrix composed of the correlation coefficient among all of the columns of $\mathbf{X}$.

Various hierarchical agglomerative clustering algorithms are then used to define groupings (clusters) of the cases based on $\mathbf{X}$. This study uses several algorithms that are frequently applied to geophysical data (Gong and Richman 1995), including three variations of the

''average linkage'' technique and the ''minimum variance'' method (Ward's method) (DeGaetano 1996). There are many objective rules that can help the user in determining the number of clusters (see DeGaetano 1996). Despite that, none is accepted as follproof or superior under a range of applications; hence, some subjectivity is required. In this study, the algorithm is stopped before it combines clusters that have clear distinctions based upon a visual inspection of the associated members. This is justified since the field of ϕ and its spatial variability tends to be smooth, and thus, it is unlikely that any true number of clusters exists (DeGaetano 1996). Accordingly, there are a number of potentially meaningful solutions that depend on the level of detail desired in the solution (Fovell and Fovell 1993).

Among the set of analyses, clustering is first performed using the correlation measure to help identify the distinct patterns. This measure removes the mean and variance of each case, which allows cases from different seasons to be classified into the same pattern. Hence, the composite maps based on this output represent significantly smoothed patterns with an unnecessarily large variance among the members of each composite. In order to improve the illustration of the patterns through composite maps, it is desirable to find analyses that are similar in terms of both their mean and variance. In order to reduce the variance, and thus to create a more meaningful composite, clustering using the Euclidean distance measure is then applied to the analyses in each pattern. Euclidean distance is frequently used as a dissimilarity measure (Gong and Richman 1995), which results in an $n \times n$ symmetric matrix composed of the root of the sum of squared differences among all of the columns of $\mathbf{X}$. This helps to better identify the cases with similar grid-averaged ϕ and variance across the grid, which are then separated into clusters within each pattern. In this application, this two-tiered approach ultimately improves the ability to visualize the patterns, and the variability within them, over what is possible from a single stratification of the dataset.

b. Analysis results

Results suggest that a wide spectrum of flow patterns is associated with the development and early evolution of DCSs. However, the majority of the events (72%) fall into three main patterns that include a well-defined upstream trough (40%), a ridge (20%), and a zonal, low-amplitude flow (12%). Each pattern is visualized through the composite maps generated from averaging the analyses within the clusters (Figs. 6–8). The remaining cases (28%) exhibit either large-scale hybrid patterns that are combinations of the three main patterns or unclassifiable patterns. The section below focuses on the characteristics of the three main patterns.

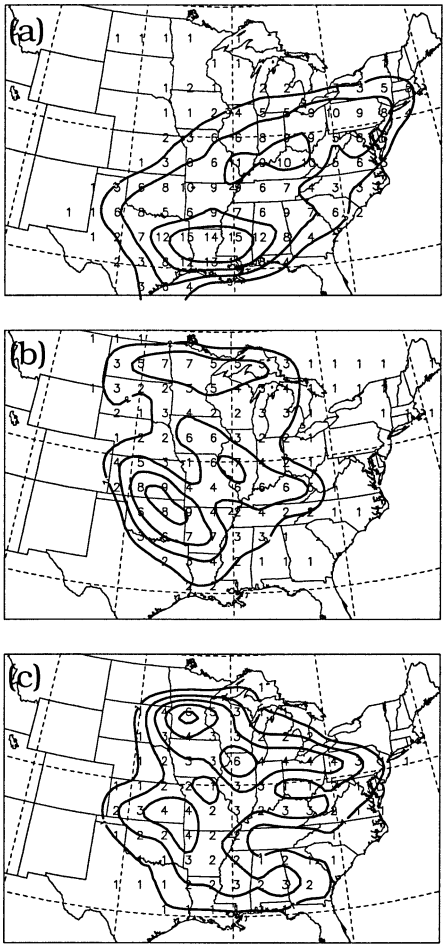

FIG. 4. The total number of derechos in 200 km $\times$ 200 km squares for (a) the 91 cases in the upstream-trough pattern, (b) the 46 cases in the ridge pattern, and (c) the 28 cases in the zonal pattern. Contours are drawn every three events in (a), every two events in (b), and every one event in (c).

1) UPSTREAM-TROUGH PATTERN

The upstream-trough pattern is formed from 91 cases (40.4%) that have a well-defined mobile upstream trough as the primary influence on the development of the DCS. The mean midlevel differential vorticity advection (estimated from the reanalysis data) is found to be 4–6 times larger for the upstream-trough events than for the ridge and zonal-flow events. Accordingly, these events best match Johns's (1993) strong-forcing/dynamic pattern and mostly exhibit characteristics of serial derechos. The upstream-trough events occur most frequently along the Gulf coast states, with a secondary activity corridor from the mid-Mississippi valley region through the lower Ohio valley (Fig. 4a). The upstream-trough events occur throughout the year (Fig. 5), with the majority of the events residing in the colder months. Notice that while many events occur in May, many of these events occur in the first half of May under ''cold season''–like conditions. This shows that while the dy-

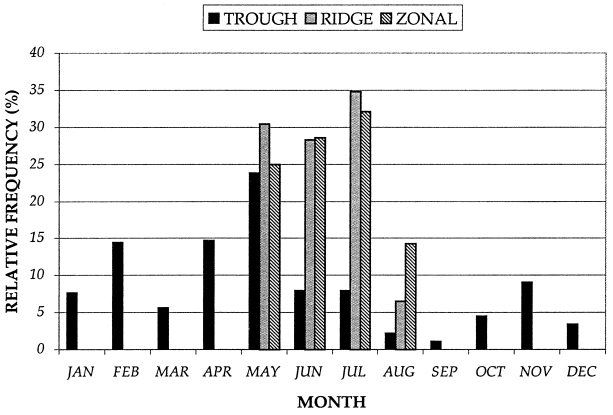

FIG. 5. The relative frequency distributions of the derecho month of occurrence among the upstream-trough, ridge, and zonal patterns.

namic pattern (and the serial derecho) is not rare during the warm season (20% occur in June–August), it is typically a cold-season pattern.

Four main clusters are identified that include 70 out of the 91 events (77%) from the upstream-trough pattern. The first upstream-trough cluster illustrates a very high-amplitude trough west of the DCS location (cluster 1 in Fig. 6a). Clusters 2 and 3 in Fig. 6a illustrate two additional upstream-trough clusters that are distinguished by progressively higher mean heights, a lessening of the mean trough amplitude, and a decrease in the 500-mb wind speed. These two clusters illustrate the most common type of upstream-trough event (see Duke and Rogash 1992; Funk et al. 1999 for examples). The remaining cluster is formed from seven warm-season upstream-trough events, with a seasonally strong, positively tilted trough propagating through a mean westerly flow. Notice that within each cluster, the mean 500-mb winds are strongest near the DCS location, indicating that the DCS often develops in the vicinity of a midlevel jet propagating around the base of the trough.

A southerly wind maximum is found ahead of a large-scale thermal boundary at 850 mb in the upstream-trough pattern (Fig. 6b). Low-level cyclogenesis is well under way in many of the colder-season events (mostly clusters 1 and 2), as the warm advection is maximized to the north and east of the DCS location. A well-defined 850-mb moisture axis lies along the axis of maximum wind ahead of the thermal boundary, which suggests that large-scale moisture transport occurs for many hours prior to the development of these cases. In addition, the mean low-level jet axis is oriented at a relatively small angle to the mean mid- and upper-level jet, which is characteristic of a pattern that may differentiate derecho occurrences from tornado outbreaks (Johns 1993). A thermal ridge becomes more evident to the southwest of the DCS location as the mean trough decreases in amplitude. This is especially apparent in cluster 4 in which the thermal boundary appears to now be oriented from west-northwest to east-southeast, with the maximum of warm advection returning to the location of DCS development. Cluster 4 shows a moisture axis extending from the south, as in clusters 1–3, but also shows a secondary axis extending east along the thermal boundary.

The left-exit region of a strong upper-level jet, and the associated divergence, are often located near the DCS location in cluster 1 (Fig. 6c). This also is found for cluster 2, with a broad region of upper-level divergence near the DCS location that can be associated with either the polar jet or the subtropical jet. Combined with the strong south-southwesterly flow and the mean frontal position at 850 mb (Fig. 6), this provides a favorable environment for the coupling of upper-level and lower-level jets, which has long been identified as a contributor to severe weather outbreaks (Uccellini and Johnson 1979). The increasing influence of the polar jet is seen for cluster 3 as the mean jet has shifted to the northeast, although the subtropical jet is still present in a few of these cases. The 250-mb jet is considerably weaker for the cases in cluster 4 and does not show a preferred location, although the mean pattern still displays a broad region of divergence just upstream of the DCS development region.

2) RIDGE PATTERN

The ridge pattern is formed from 46 events (20.4%) that are influenced by the anticyclonic flow around a ridge at 500 mb. These cases best match Johns's (1993) warm-season pattern and all exhibit characteristics of progressive derechos. The ridge pattern events occur in three distinguishable regions: one stretching northwest to southeast across the southern Great Plains, one stretching west-northwest to east-southeast from Iowa to Kentucky, and another stretching west to east from the northern plains to the western Great Lakes region (Fig. 4b). The 46 ridge events all occur during the warm season (Fig. 5).

Three main clusters are identified in the ridge pattern that include 31 out of the 46 cases (67%). The first cluster contains nine events that develop upstream of the ridge axis. The mean pattern displays a short-wave trough in the process of breaking down the northern extent of the strong ridge. This produces a mean 20–25 m s^{-1} 500-mb jet just to the north of the DCS location (Fig. 7a). All of the cases in this cluster develop in the northern plains region (not shown) and are long-lived events. An example is the particularly destructive derecho event on 4–5 July 1999 that developed in South Dakota and decayed many hours later off the coast of Maine (Miller and Johns 2000). The second cluster identifies 10 events that develop near the axis of a flat ridge with a weakly confluent zonal flow to the north (cluster 2 in Fig. 7a) (see Evans and Corfidi 2000 for an example). The mean 500-mb wind speed is weakest for this cluster, with values of 15–18 m s^{-1} near the location of DCS development. The third cluster identifies 12

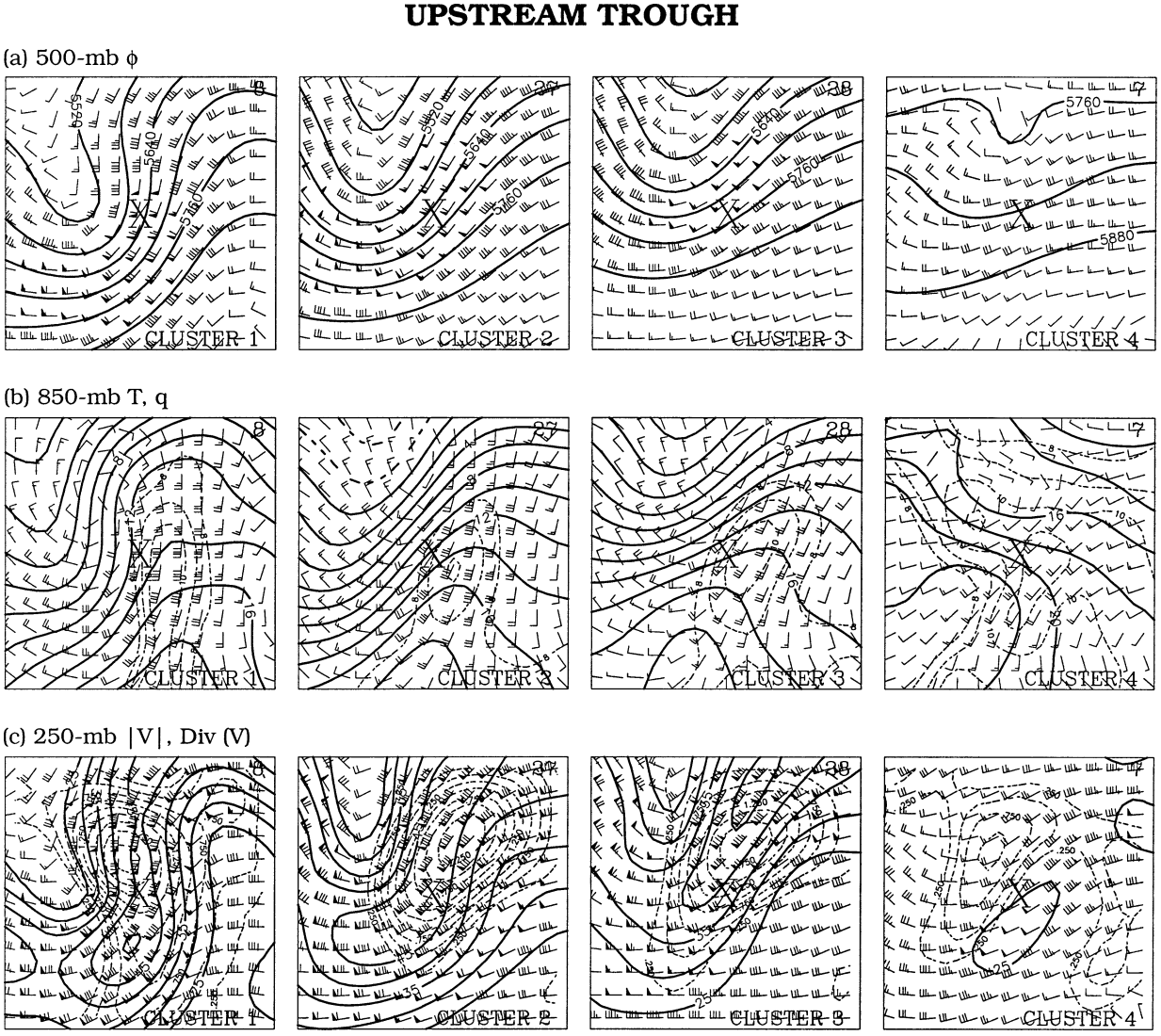

FIG. 6. (a) The mean 500-mb geopotential height (ϕ, contours every 60 m) and wind (flag, 25 m s^{-1}; full barb, 5 m s^{-1}) for four clusters within the upstream-trough pattern. (b) As in (a) except for the 850-mb temperature (T, solid contours every 2 K) and specific humidity (q, dashed contours every 1 g kg^{-1} starting at 8 g kg^{-1}). (c) As in (a) except for the 250-mb wind speed [$|V|$, solid contours every 5 m s^{-1}, starting at 25 m s^{-1} and divergence of the wind Div (V), dashed contours every 0.25 $\times$ 10^{-5} s^{-1}]. The horizontal and vertical dimensions of each grid are 2600 km by 2400 km, respectively. The X denotes the mean position of the DCS at the analysis time. The number in the upper-right corner of each grid denotes the number of analyses in each composite (cluster).

events that develop downstream of a high-amplitude ridge within mean 500-mb northwesterly flow of 16–20 m s^{-1} (see Miller et al. 2002 for an example). Many of these cases display a weak, short-wave trough digging southeast downstream of the ridge, which produces stronger flow in the vicinity of and to the northeast of the DCS location.

The patterns of 850-mb temperature for the ridge pattern (Fig. 7b) qualitatively resemble their associated patterns of 500-mb heights, with a thermal boundary oriented parallel to the mean midlevel flow. This is a sign that the midlevel large-scale flow is often equivalent barotropic (Bluestein 1993) and is a sign that the large-scale forcing is often provided through low-level warm advection. As identified by Johns et al. (1990), a common thread to these events is that the warm advection becomes progressively weaker downstream. An axis of 850-mb moisture along the thermal boundary near and downstream (relative to the midlevel flow) of the DCS location is clearly evident in this pattern, which is another important feature originally identified by JH87 and Johns et al. (1990).

An interesting finding is that the right-entrance region of a strong polar jet is usually located near the DCS for the cases within this pattern. In addition, a comparison of Figs. 8a and 8c shows that the mean wind speed in-

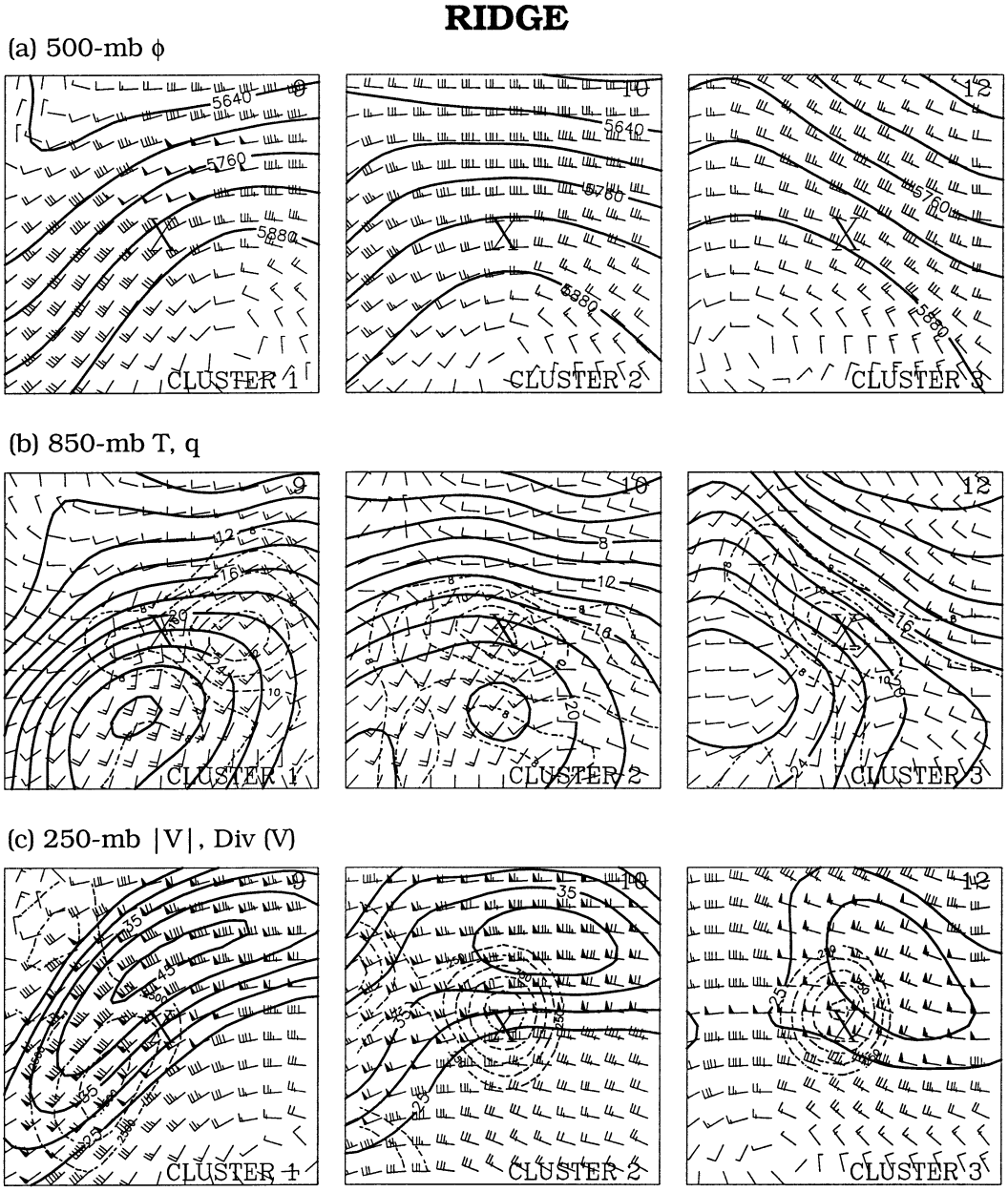

FIG. 7. As in Fig. 6 except for the ridge pattern.

creases by as much as 20–25 m s^{-1} from 500 to 250 mb near the location of DCS development. Although the mesoscale details are beyond the scope of this paper, these two factors produce a favorable scenario for the development of ageostrophic, thermally direct circulations related to jet stream disturbances (Bluestein 1993). It is likely that these jet stream circulations augment the forcing provided by low-level warm advection in many of the events. The jet is strongest for the cases in cluster 1, with 250-mb wind speeds as high as 40–45 m s^{-1} just to the north of the DCS location. The prevalence of the right-entrance region of the jet is also evident in clusters 2 and 3, with the maximum of divergence almost exactly collocated with the location of DCS development.

3) ZONAL PATTERN

The zonal pattern contains 28 events (12.4%), mostly progressive derechos, that identify an additional warm-season pattern that has not been emphasized in previous literature (Fig. 5; see Spoden et al. 1996 for an example). The zonal flow events tend to occur most frequently from the upper Midwest through the lower Great Lakes

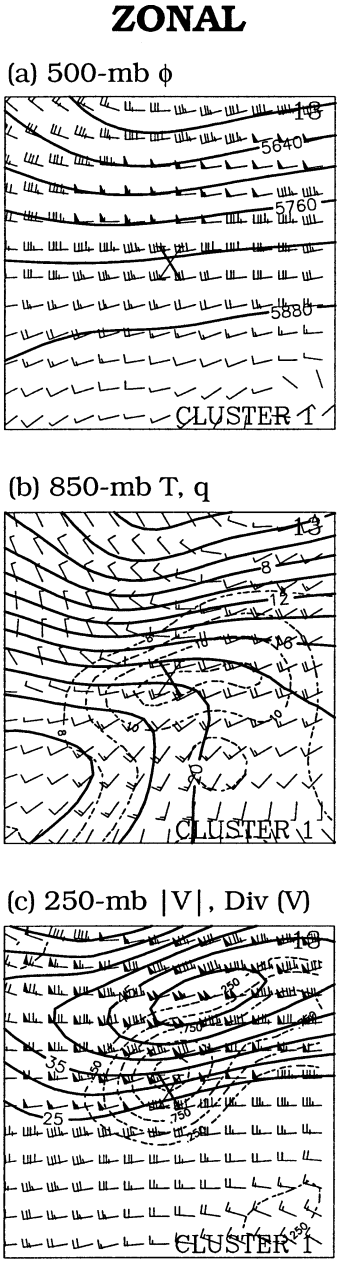

FIG. 8. As in Fig. 6 except for the zonal pattern.

region, but also occur in the eastern plains and the Gulf coast states (Fig. 4c).

The composite maps from a cluster of 13 events show a strong mean midlevel flow of 25–30 m s^{-1} just to the north of the DCS location (Fig. 8a). Despite the lack of an identifiable midlevel trough in the mean flow, a trough axis is evident at 850 mb, which extends southwest to northeast upstream of the DCS location (Fig. 8b). A mean southwesterly 850-mb flow of approximately 10 m s^{-1} extends ahead of this trough and lies along a thermal ridge axis to the south and west. A strong east–west-oriented thermal boundary lies near and to the north of the DCS location, with a zone of warm advection and an axis of moisture that stretches near and downstream of the DCS location. As in many of the ridge cases, an unseasonably strong 250-mb jet (shown with a mean speed $>$50 m s^{-1}) lies to the north of the DCS location and places the development region in its associated divergence. This indicates the frequent existence of jet streaks propagating through the mean flow and the possibility of thermally direct circulations that aid in the development of the systems.

c. Discussion

It should be emphasized that the individual cases within each cluster necessarily display a degree of variability on scales resolved by the reanalysis data that is inherent in the choice of detail allowed in the clusters. As an example, the individual analyses that compose cluster 1 of the upstream-trough pattern are shown in Fig. 9. These analyses display similarities in terms of the direction and speed of the midlevel flow, as well as the mean pattern and magnitude of the heights, but show some variability in the shape and position of the trough. This large-scale variability is in addition to important mesoscale details that are often superimposed on the main flow pattern (Pryzbylinski 1995; Bosart et al. 1998; Klimowski et al. 2000), but are not considered in this analysis.

Forecasters should also be made aware that large-scale hybrid patterns and some unclassifiable patterns account for the remaining 28% of the events. The hybrids combine various characteristics of the three main patterns and mainly occur in the warm season (three examples are shown in Fig. 10). The existence of these other patterns and the variability within each pattern shows that the idealized dynamic and warm-season patterns discussed by Johns (1993) only depict a portion of the full spectrum of the possibilities of large-scale flow patterns associated with the development of DCSs. Despite these complicating factors, since 72% of the cases tend to show characteristics of only three broad, large-scale flow regimes, it is believed that the composite maps can assist forecasters through the improved visualization of the most common patterns and the potential physical mechanisms responsible for the development of DCSs. While knowledge of the typical large-scale patterns is important in terms of pattern recognition techniques, the vertical structure of the atmosphere also is crucial in the application of ingredients-based forecasting techniques (Johns and Doswell 1992). Thus, we now explore the vertical structures of DCS environments using soundings.

4. Proximity soundings

In this section, the environments of DCSs are examined with the use of proximity soundings. While we recognize the problems of utilizing the operational sounding data in this manner (Brooks et al. 1994), these data still provide the best and most widely available source of si-

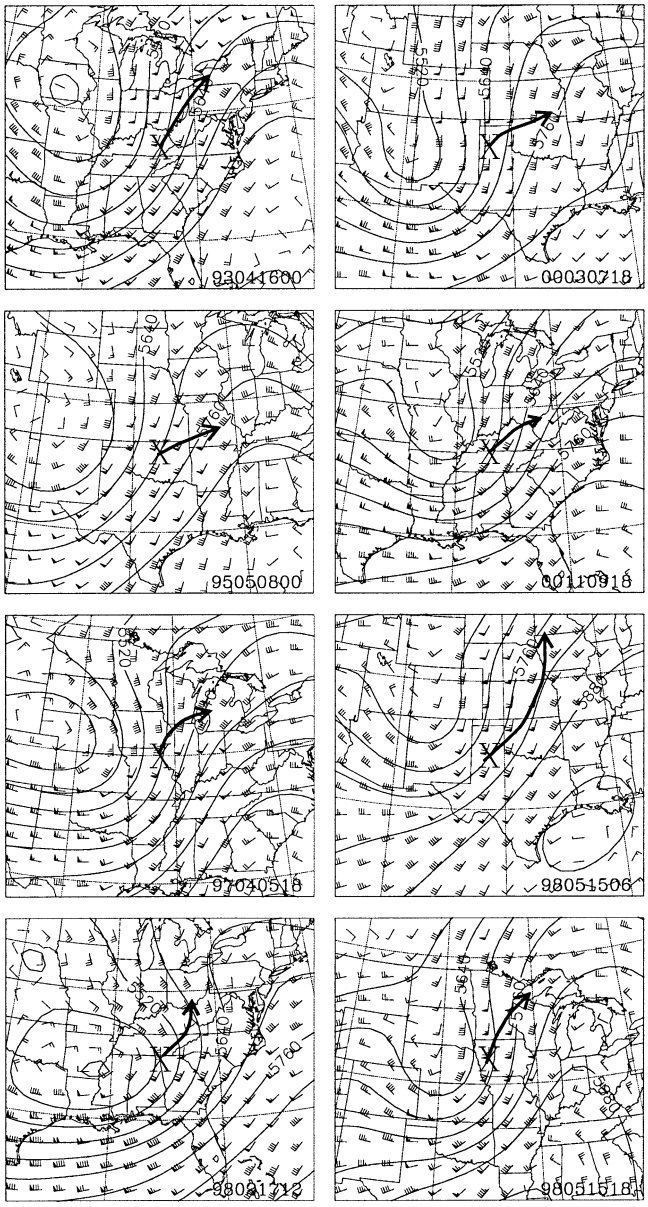

FIG. 9. The 500-mb geopotential height and wind (as in Fig. 6) for the eight cases that compose cluster 1 in the upstream-trough pattern. The X denotes the approximate location of the DCS at the analysis time and the arrow depicts the approximate track of the derecho major axis. The time of each analysis (UTC in YYMMDDHH format) is displayed in the lower right of each panel.

multaneous wind and thermodynamic information. This study focuses on CAPE and the vertical distributions of wind shear and moisture, which have all been emphasized as important contributors to severe-wind-producing convection (JH87; Atkins and Wakimoto 1991; Bentley et al. 2000; Evans and Doswell 2001).

a. Definition and classification of the dataset

Soundings that are within 300 km of the DCS leading edge in the downshear environment are considered candidates for proximity soundings. The candidates are further restricted to those that are no more than 80 km ''north'' of the derecho major axis and no more than 200 km ''south'' of the derecho major axis plotted in a coordinate system relative to the DCS motion. Using hourly radar and surface data as guidance, soundings that are either too close to the convection or are obviously contaminated by the convection are removed. Soundings that sample convective outflows or drylines in low levels, but appear uncontaminated otherwise, also

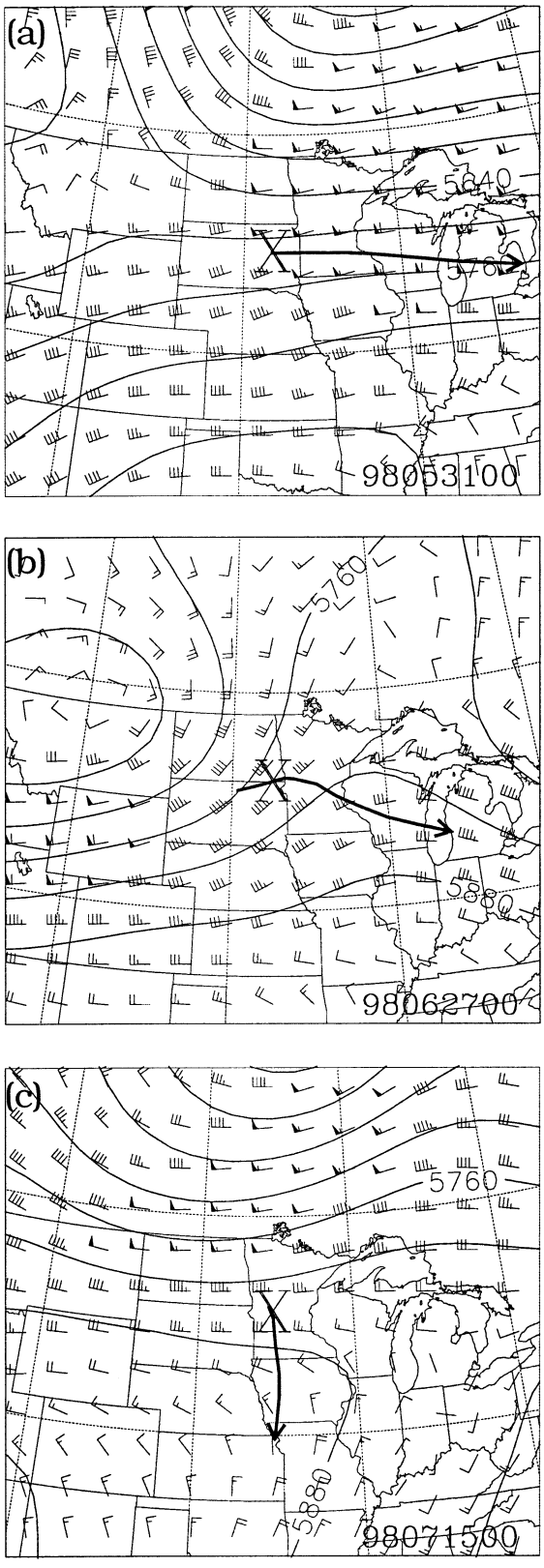

FIG. 10. Examples of 500-mb geopotential heights and winds from hybrid patterns. (a) An example of an upstream-trough–zonal pattern hybrid. (b) An example of an upstream-trough–ridge pattern hybrid. (c) An example of an unclassifiable hybrid pattern. The approximate track of the derecho major axis is depicted by the arrow. The time of each analysis (UTC in YYMMDDHH format) is displayed in the lower right of each panel.

are discarded. Finally, only soundings that have mandatory and significant level wind data up to at least 10 km are retained. This procedure identifies 168 proximity soundings.

Sounding parameters are first examined relative to the life cycle of the DCS. Similar to the methodology outlined in section 3 for the normalization of the flow patterns, the observation time for each sounding is normalized and grouped into 38 ''beginning'' ($t \leq 0$), 52 ''mature'' ($0 < t < 0.5$), and 78 ''decay'' ($t \geq 0.5$) soundings.

The sounding parameters also are examined relative to the synoptic-scale forcing for upward motion as a means to stratify the parameters among the different regimes. The stratification is defined empirically using the maximum 500-mb **Q**-vector divergence ($\nabla\cdot\mathbf{Q}$) (in the reanalysis data) within 500 km of the DCS location as guidance. The soundings for which $t < 0.5$ are categorized into 27 ''strong forcing'' ($\nabla\cdot\mathbf{Q} \leq -10 \times 10^{-16}$ kPa m^{-2} s^{-1}), 27 ''moderate forcing'' (-10×10^{-16} kPa m^{-2} s^{-1} $< \nabla\cdot\mathbf{Q} < -5 \times 10^{-16}$ kPa m^{-2} s^{-1}), and 37 ''weak forcing'' soundings ($\nabla\cdot\mathbf{Q} \geq -5 \times 10^{-16}$ kPa m^{-2} s^{-1}). As a consequence of these thresholds for $\nabla\cdot\mathbf{Q}$, all of the 37 weak-forcing soundings are confined to the months of May–August while only 9 of the 27 strong-forcing soundings occur during these months (Fig. 11). All but three of the moderate-forcing soundings occur in the warm season. This helps to illustrate that the strong-forcing soundings generally represent the upstream-trough pattern identified in the previous section, while the weak-forcing soundings generally represent the ridge and zonal-flow patterns. Over half of the moderate forcing soundings represent various hybrid patterns.

b. Proximity sounding results

1) LIFE CYCLE STRATIFICATION

The most significant difference[3] in the CAPE distributions is between the beginning and decay soundings (Fig. 12). The mean CAPE drops from 2742 J kg^{-1} for the beginning soundings to 1451 J kg^{-1} for the decay soundings. Also notice that 90% of the beginning sound-

[3] Differences between the various subsets are tested for statistical significance using a two-tailed Student's *t* test based on the sample means and standard deviations (Wilks 1995). When possible (sample sizes ≥ 25), differences are considered significant if the chance that the two sample means originate from different distributions is $\geq$95%.

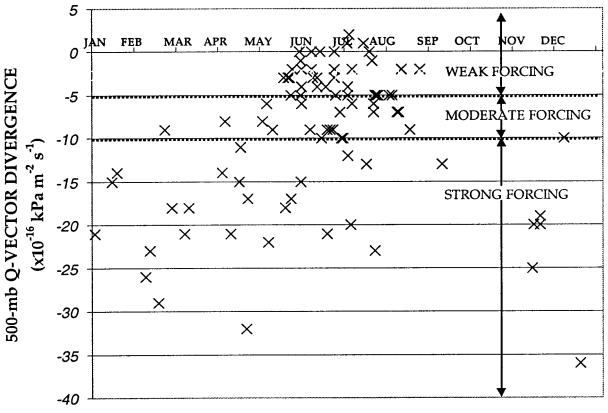

FIG. 11. The distribution of the mean 500-mb **Q**-vector divergence (scaled by 10^{16} kPa m^{-2} s^{-1}) vs day associated with the 91 beginning and mature proximity soundings. The thresholds for defining the forcing stratification are shown by the dashed lines.

ings have CAPE above 1000 J kg^{-1}, whereas 40% of the decay soundings have CAPE below 1000 J kg^{-1} (Fig. 12). Large amounts of instability are frequently found in the initial environments as nearly 50% of the beginning soundings have CAPE above 2500 J kg^{-1}. This suggests that a decrease in instability is potentially a significant factor in the demise of DCSs.

Past studies identify the environmental relative humidity (RH) profile as a potentially significant factor in the development and maintenance of strong downdrafts within thunderstorms. Low environmental RH in midlevels aids the initiation of downdrafts by precipitation phase changes (Hookings 1965; Gilmore and Wicker 1998). However, Srivastava (1985) and Proctor (1989) suggest that higher environmental RH in the underlying layer of parcel descent supports the maintenance of strong downdrafts. Given a sufficiently steep lapse rate, the higher moisture content increases the virtual temperature of the environment, which leads to larger virtual temperature differences between the environment and the parcel.

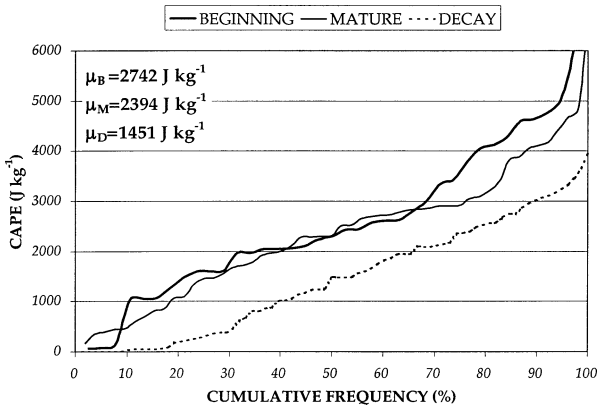

FIG. 12. The cumulative frequency distribution of CAPE (J kg^{-1}) for the beginning, mature, and decay soundings. The sample means for the beginning (μ_B), mature (μ_M), and decay (μ_D) soundings are shown in the upper left-hand corner. Note that μ_D is significantly different than both μ_B and μ_M at the 95% confidence level.

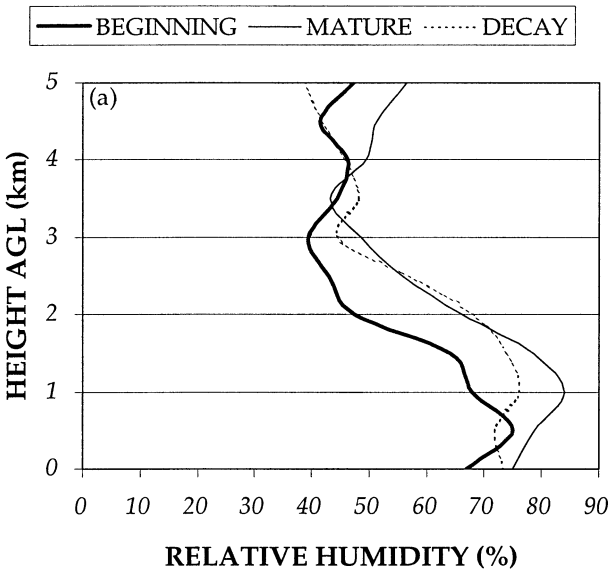

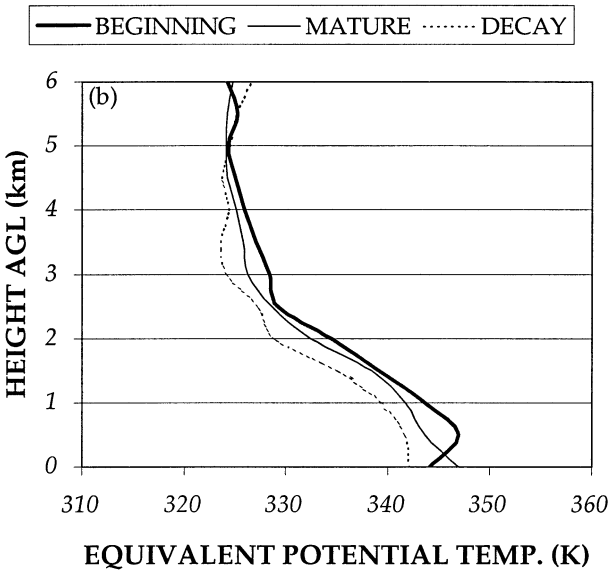

FIG. 13. Vertical profiles of (a) median RH and (b) θ_e for the beginning, mature, and decay soundings. The beginning and mature RH profiles are statistically different at the 95% confidence level between 1 and 2.5 km. There are no statistically significant differences in the θ_e profiles.

The RH varies considerably during all stages of the DCS life cycle, but insight is gained by examining the median profiles. The largest differences are between the beginning and mature soundings and are statistically significant in the 1.0–2.5-km layer. The vertical difference in median RH is largest for the mature soundings with median values near 85% at 1 km that drop to 42% near 3.5 km (Fig. 13a). This suggests that DCSs tend to mature as they move into moister low-level environ-

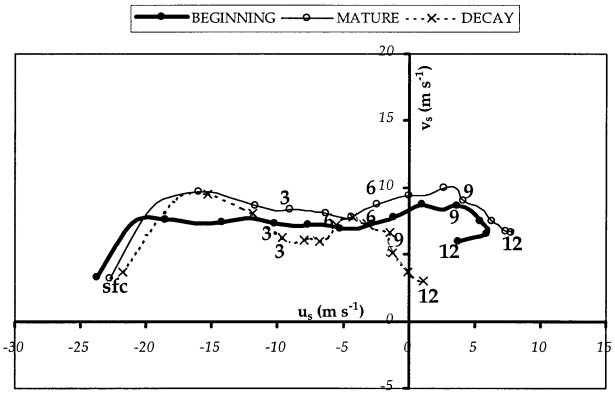

FIG. 14. Mean hodographs for the beginning, mature, and decay soundings. Prior to averaging, the wind components (u, v) in each sounding are represented in a coordinate system with the tip of the mean MCS motion vector (u_s, v_s) at the origin. The mean winds are calculated every 0.5 km AGL, are plotted every 1 km AGL, and are labeled every 3 km AGL. Mean shear values related to the mean hodographs are given in Table 1.

TABLE 1. Mean 0–1-, 0–2.5-, 0–5-, and 5–10-km shear vector magnitudes (m s^{-1}) for the life cycle stratification (beginning, mature, decay) and the forcing stratification (strong, moderate, weak). Italic valued cells in the life cycle stratification indicate that the sample mean is statistically different than the sample mean for the decay soundings at the 95% confidence level. Italic valued cells in the forcing stratification indicate that the sample mean is statistically different than the sample mean for the weak-forcing soundings at the 95% confidence level.

State	0–1 km	0–2.5 km	0–5 km	5–10 km
Beginning	8.7	14.1	*20.4*	*14.3*
Mature	10.6	15.0	*20.3*	13.6
Decay	9.9	13.2	16.6	11.6
Strong	*15.3*	*18.3*	*23.8*	15.6
Moderate	8.4	15.1	19.0	11.3
Weak	6.8	11.4	18.8	14.4

ments, while still maintaining relatively dry conditions above 3 km. This result is in general agreement with those of Srivastava (1985) and Proctor (1989) and suggests that relatively dry midlevels combined with low-level moistening ahead of a developing MCS signals the increasing potential for downdraft and strong surface wind production.

The low levels tend to dry somewhat toward decay, which reduces the vertical RH gradient and is likely a factor in the reduced CAPE for the decay soundings (Fig. 12). However, this difference is not statistically significant, which implies that a relatively drier low-level environment ahead of a mature DCS often does not signal its decay.

The beginning and mature soundings both display a vertical decrease in the median equivalent potential temperature (θ_e) of $>$20 K (Fig. 13b). Overall, the vertical decreases in θ_e appear to be even larger for DCSs than for those reported for strong downdrafts within more isolated convective cells by Atkins and Wakimoto (1991) (the next section shows that the more weakly forced events are largely responsible for this large convective instability). The tendency for DCSs to develop north of a low-level thermal boundary (JH87) is indicated by the low-level inversion in the median θ_e profile for the beginning soundings (Fig. 13b). The fact that this inversion is not evident for the mature soundings (Fig. 13b) indicates that the systems tend to move toward the warm sector as they mature (JH87). The low-level θ_e decreases slightly toward decay (Fig. 13b), but this difference is not statistically significant. This suggests that low-level θ_e, along with the low-level RH, is not necessarily a useful indicator of DCS decay, which appears to be the case for MCSs in general (Gale et al. 2002).

The mean hodographs display a unidirectional shear profile (''straight line'') and significantly weaker deeper-layer shear for the decay soundings (Fig. 14). In many events, this decrease in deep shear is the result of the propagation away from the mid- to upper-level jet. The mean 0–5-km shear drops from over 20 m s^{-1} for the beginning and mature soundings to 16.6 m s^{-1} for the decay soundings (Table 1). Likewise, the mean 5–10-km shear drops from 14.3 m s^{-1} for the beginning soundings to 11.6 m s^{-1} for the decay soundings (Table 1). The mean low-level shear (0–1 and 0–2.5 km) shows no significant differences in the DCS life cycles (Table 1). Gale et al. (2002) found similar results for general warm-season MCSs. This adds observational support to the conclusions of Coniglio and Stensrud (2001) that DCSs can be maintained by system-scale circulations that are favored by deep-tropospheric shear and convergence along the gust front (Moncrieff 1992; Shapiro 1992; Moncrieff and Liu 1999).

It should be noted that some of the more weakly forced events do show a decrease in the low-level shear toward decay, and thus the persistence of the overall mean low-level shear toward decay is ascribed to the strong low-level shear observed for the strongly forced soundings (shown later). Similarly, examination of Fig. 14 suggests that the low-level storm-relative inflow appears to persist toward decay. However, the length of the hodograph for the beginning and mature soundings is ascribed to the strong low-level winds observed in the strongly forced soundings (shown later). The storm-relative inflow does show a decrease toward decay for the more weakly forced events (not shown). However, the sample sizes are insufficient to break down each life cycle classification by forcing regime, and thus the significance of these details cannot be determined.

2) FORCING STRATIFICATION

The cumulative frequency distributions of CAPE (Fig. 15) show a distinct separation between the strong-forcing (SF) soundings and the moderate-forcing (MF) and weak-forcing (WF) soundings (again, only the soundings with $t < 0.5$ are included). All but two of

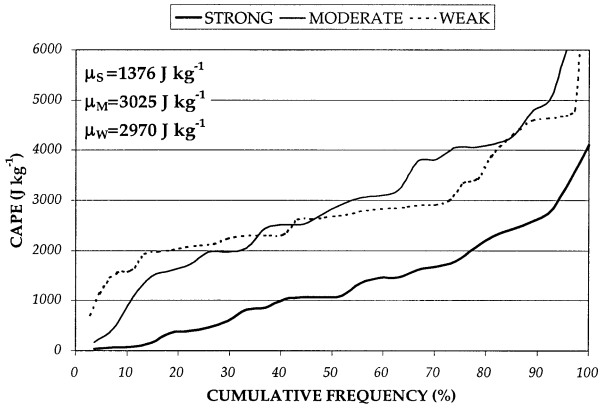

FIG. 15. The cumulative frequency distribution of CAPE (J kg^{-1}) for the strong-, moderate-, and weak-forcing soundings. The sample means for the strong- (μ_S), moderate- (μ_M), and weak- (μ_W) forcing soundings are shown in the upper-right corner. Note that μ_S is significantly different than both μ_M and μ_W at the 95% confidence level.

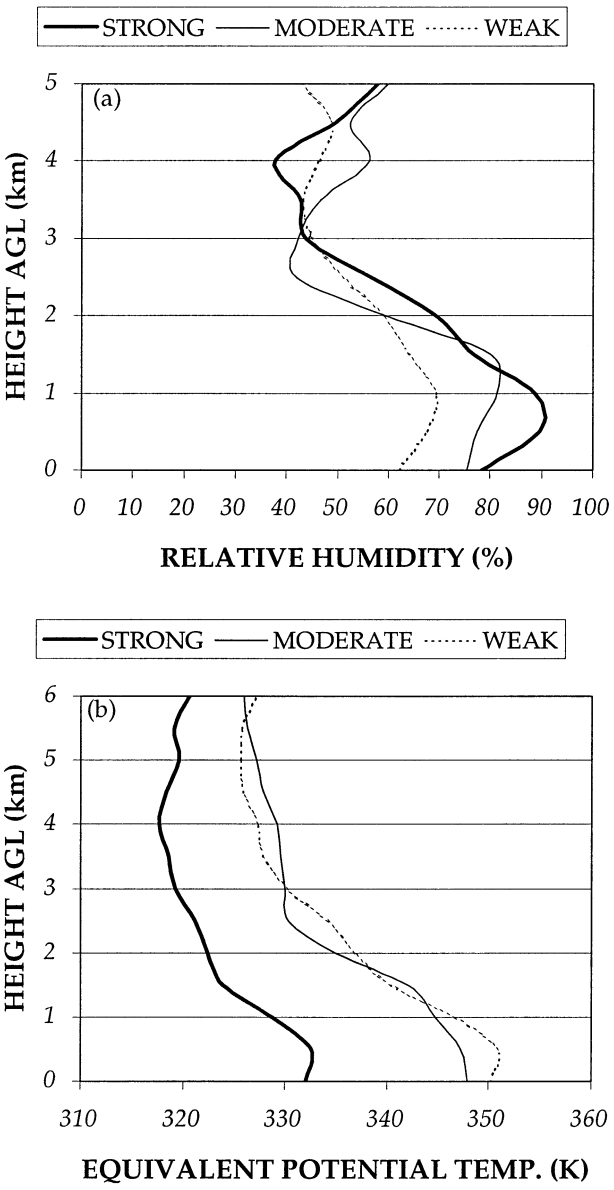

FIG. 16. As in Fig. 13 except for the strong-, moderate-, and weak-forcing soundings. The strong- and weak-forcing profiles are statistically different at the 95% confidence level between the surface and 1.25 km. The strong forcing θ_e profile is significantly different from the moderate- and weak-forcing θ_e profiles at the 95% confidence level at all vertical levels (0–6 km).

the WF soundings have CAPE above 1000 J kg^{-1}, while almost 50% of the SF soundings have CAPE below this amount. Extreme instability also is noted for the WF and MF soundings with almost 50% having CAPE above 2700 J kg^{-1}. Soundings with extreme instability appear to be very rare under strong forcing, which appears to be largely due to their prevalence during the cold season, but also could be due to the tendency for high-CAPE–strong-shear environments to support supercells (Johns and Doswell 1992).

As for the examination of RH among the various DCS life cycles, significant differences are found in the median profiles. For the SF soundings, the median RH reaches a maximum near 90% at 0.75 km and drops to a local minimum of 38% at 4 km. As discussed previously, this large vertical RH gradient translates into a significant potential for downdraft production. It also has been recognized that a reduction in the environmental lapse rates within the downdraft layer lessens the potential for maintaining downdrafts (Hookings 1965; Srivastava 1985; Proctor 1989). Relatively modest environmental lapse rates are observed for the SF soundings, which is apparent in the relatively small CAPE values (Fig. 15) and the relatively small vertical decrease in median θ_e for the SF soundings (Fig. 16b). This suggests that the dramatic vertical RH gradient observed for the SF soundings, and the associated increased potential for downdraft production (Proctor 1989), perhaps counter a decreased potential for downdraft production associated with rather modest lapse rates. A dramatic vertical RH gradient is, therefore, a possible reason for why derechos can occur with low CAPE.

While the vertical decrease in median RH becomes progressively smaller for the MF and WF soundings (Fig. 16a), the vertical decrease in θ_e becomes progressively larger, with the median profile showing a vertical decrease of ~24 K from the low to midlevels (Fig. 16b). This affirms that WF events tend to have large values of convective instability in the environment.

Unlike the life cycle stratification, the most significant differences in shear are found in the low-level shear parameters (Fig. 17 and Table 1). For example, the mean 0–2.5-km shear drops from 18.3 m s^{-1} for the SF soundings to 11.4 m s^{-1} for the WF soundings (Table 1). The shear component normal to the DCS motion vector in the lowest 2 km (Fig. 17) contributes a significant amount to this large mean low-level shear for the SF

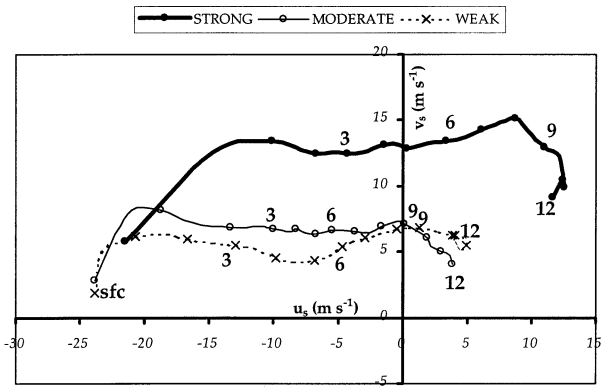

FIG. 17. As in Fig. 14 except for the strong-, moderate-, and weak-forcing soundings. Mean shear values are given in Table 1.

soundings (Table 1) and is likely produced by the strong low-level jets that frequently occur in this forcing regime (Fig. 6). Mean 5–10-km shear values of 11–16 m s^{-1} with a large range of values (3–40 m s^{-1}) show that the shear very often extends throughout the depth of the troposphere, regardless of the forcing regime.

Strong near-surface inflow is noted among all three forcing regimes, but the variations in vertical shear result in differences in the depth and orientation of the inflow layer. For the SF soundings, the mean top of the inflow layer ($u_s = 0$) is found near 5 km. A positive u_s above 5 km combined with a strong mean wind component normal to the DCS motion vector likely contributes to the parallel or leading stratiform precipitation (Parker and Johnson 2000) that is usually observed among these events. This also shows that the majority of the low-level inflow originates normal to, and to the right of, the mean DCS motion vector (which is usually from the south and southeast of the DCS).

For the MF and WF soundings, the mean top of the inflow layer increases to between 8 and 9 km. The rearward flow in midlevels likely contributes to the frequent appearance of these events as asymmetric, trailing-stratiform MCSs (Houze et al. 1989; Parker and Johnson 2000). In addition, the relative low-level inflow originates from a direction that is at a large angle (140°–160°) to the mean DCS motion vector. This allows the system to ingest the high-θ_e low-level air in the downshear environment (Figs. 8b, 9b, and 17b). This also contributes to very strong storm-relative inflow integrated over the lowest 3 km. The existence of mean 0–5-km shear of 18–20 m s^{-1} produces considerably weaker midlevel (5–7 km) storm-relative flow (Fig. 18). This supports one of the key findings of Evans and Doswell (2001) that DCSs with weak synoptic-scale forcing tend to form in such environments that support the fast-forward propagation of the cold pool.

3) COMPARISON TO SIMULATIONS

Using a horizontally homogeneous cloud-scale numerical model, Weisman (1993) produces a comprehensive set of simulations of convective systems that include structures resembling observed DCSs. One of the goals of Weisman (1993) was to identify the minimum thresholds of CAPE and shear within the idealized simulations that produce these structures and to compare them to environmental conditions associated with observed severe long-lived bow echoes. The present comprehensive observational dataset affords a detailed comparison of this type and is presented in light of its relevance to forecasting severe, long-lived bow echoes.

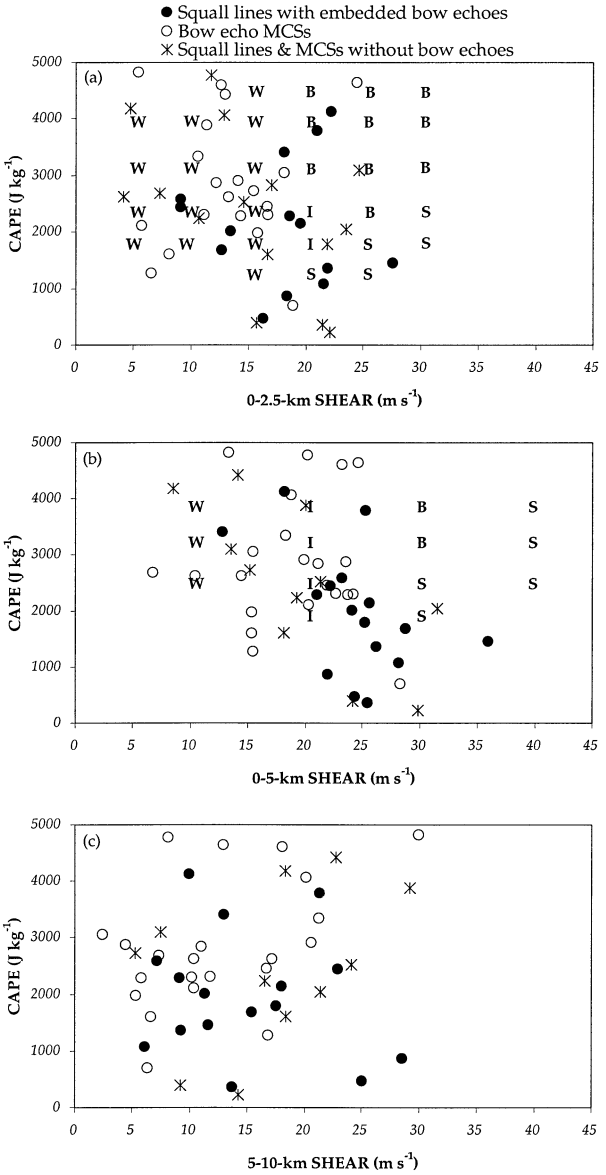

FIG. 18. Scatterplots of (a) 0–2.5-, (b) 0–5-, and (c) 5–10-km shear vector magnitudes (m s^{-1}) vs CAPE (J kg^{-1}) for those soundings in which the convective structure of the DCS is identified (see legend at top of figure). Results from Weisman's (1993) numerical simulations of convective systems also are shown in (a) and (b) (see his Fig. 24). The letters represent the convective structures of the simulated systems as defined by Weisman (1993).

Weisman (1993) subjectively defines the structure of the simulated convective systems into three main categories. The first category includes systems with weak cells tens of kilometers behind the leading edge of the gust front (*W*), in which structures resembling strong, long-lived bow echoes do not develop. The second category includes strong, long-lived bow-echo structures with a pronounced rear-inflow jet and cyclonic vorticies along the ends of the bow (*B*). The third category includes strong, isolated cells, some supercells, scattered along the gust front (*S*), with no indications of larger-scale rear inflow that composes the bow-echo cases. A fourth intermediate category (I) is defined that contains attributes of both the *W* and *B* cases. Weisman finds that the well-defined bow-echo simulations are generally restricted to environments with shear greater than 20 m s^{-1} and are favored if this shear is entirely confined to the lowest 2.5 km.

To compare the present observations to these simulations, WSR-88D mosaics at 2- or 4-km resolution or, when available, the level II WSR-88D data, are used to define a typical convective structure for each event that has a beginning or mature proximity sounding. Due to the lack of sufficient radar data for the majority of the events, it is possible to adequately define a convective structure for only 53 of these events. DCSs that contain well-defined bow echoes for at least a 1-h period and resemble the *B* simulations in Weisman (1993) are identified. In addition, DCSs that show either short-lived bow echoes, or none at all, and resemble the *W* simulations from W93 also are identified. Each case also is defined as having either elongated squall-line characteristics with parallel or leading stratiform precipitation or as having characteristics more typical of trailing-stratiform MCSs.

The results show that the vast majority of the soundings that sample bow-echo squall lines or bow-echo MCSs have 0–2.5-km shear outside the range of values that produce the B simulations from Weisman (1993) (Fig. 18a). In fact, 14 out of the 20 soundings that sample bow-echo MCS environments (70%) have 0–2.5-km shear below 15 m s^{-1}. Most of the values from the observed bow-echo MCSs cluster around the shear environments that produce the *W* simulations (Fig. 18a), which typically do not represent the DCS structures observed in this study. This confirms the implication of Evans and Doswell (2001) that long-lived bow echoes can and often do occur in environments with low-level shear magnitudes that are less than those suggested by the Weisman (1993) simulations and that *the low-level shear may not be useful in forecasting long-lived bow-echo structures in many situations.* The results from section 4a that show no significant changes in low-level shear among the three phases of the DCS life cycle add weight to this conclusion. It should be noted that more of the observed soundings have shear values that support at least some bow-echo structures in the simulations (the I simulations) when the shear layer is extended to 5 km above ground (Fig. 18b). Only 4 out of the 20 bow-echo MCSs have 0–5-km shear less than 15 m s^{-1}. Therefore, the presence of moderate to strong unidirectional shear in the 0–5-km layer appears to be a better predictor of the potential for severe MCS structures than the low-level shear.

It should also be noted that the simulations do not represent the several observed bow-echo squall lines that occur with strong low-level shear and CAPE $<$ 1000 J kg^{-1}. These cases appear to be supported more from stronger synoptic-scale forcing that is not well represented in the idealized simulations.

Weisman and Rotunno (2002) update their results to include simulations with shear in a layer up to 10 km deep [the Weisman (1993) simulations only included shear in the lowest 5 km]. The simulations that include shear above 5 km do not develop long-lived bow-echo structures (they are described as either upshear-tilted multicellular systems or systems composed of isolated cells and/or embedded supercells). However, the mean 5–10-km shear observed among the well-defined bow-echo events is approximately 14 m s^{-1}, and is as large as 30 m s^{-1} (Fig. 18c). This shows that the idealized numerical simulations appear to have difficulty reproducing DCS events within deep-shear environments and further emphasizes some disparities between observations and the idealized models. Simulations using the CAPE, shear, and moisture values of observed DCSs and the associated nonhomogeneous large-scale flow patterns identified in this study need to be produced to help reconcile these disparities in observations and idealized models and to provide improved information to forecasters.

5. Summary

This study shows that there are many types of flow patterns associated with DCSs. However, from a set of 225 analyses of 500-mb geopotential heights associated with the development and early evolution of DCSs, the majority (72%) of the events can be categorized into three main patterns. The most prominent pattern consists of an upstream trough of varying amplitude (40% of the cases) that contains events from all times of the year and shows a qualitative resemblance to the dynamic pattern defined by Johns (1993). A ridge is defined as the primary large-scale feature in 20% of the cases, all of which are confined to the months of May–August. A zonal-flow pattern is defined in 12% of the cases, which defines an additional warm-season pattern than has not been emphasized in past literature. The remaining 28% of the cases form large-scale hybrid or unclassifiable patterns that contain various characteristics of the three main patterns. These results should make forecasters aware that derechos can develop under a variety of large-scale flow patterns during all months of the year and that the idealized dynamic and warm-season patterns discussed by Johns (1993) only depict a

portion of the full spectrum of the possibilities of large-scale flow patterns associated with the development of DCSs.

An analysis of a large set of proximity soundings shows that DCSs tend to mature as they move into an increasingly moist low-level environment while maintaining relatively dry conditions at midlevels. In addition, the DCSs tend to decay as they move into an environment with less CAPE and decreasing 0–5- and 5–10 km shear, but no significant differences in the 0–1- and 0-2.5–km shear (although some of the more weakly forced events show weaker low-level shear toward decay). Overall, this suggests that mature DCSs can be maintained by the larger-scale circulations that depend on the shear throughout the depth of the troposphere (see Coniglio and Stensrud 2001 for a detailed discussion).

The strong-forcing events that typify the upstream-trough pattern show the largest vertical decrease in RH, despite only a modest CAPE and convective instability. The enhancement of downdraft production from this strong vertical RH gradient perhaps explains why derechos can persist within environments of relatively low instability.

A mean, nearly ''straight-line'' hodograph with shear throughout the depth of the troposphere is common to DCSs that form within all large-scale forcing regimes. The low-level shear is found to be significantly larger for the strong-forcing events (tied to strong low-level jets) than for the more weakly forced events that typify the ridge and zonal-flow patterns. Accordingly, storm-relative hodographs show relative inflow up to about 5 km for the strong-forcing soundings and relative inflow up to almost 9 km for the weak-forcing soundings. These findings add support to Evans and Doswell (2001) who suggest that strong low-level storm-relative inflow may largely impact the strength, mode, and duration of the more weakly forced DCSs.

A comparison of the results to past idealized simulations suggests a discrepancy between observations of severe, long-lived convective systems and the environments required to simulate them in some idealized numerical models. This information is pertinent to forecasters who have real-time proximity sounding information and use results from the idealized numerical simulations as guidance. Even for the well-defined bow-echo MCSs, the observed low-level shear is usually weaker than what is required to simulate them in idealized models. These results suggest that minimum low-level shear thresholds are not useful for forecasting severe MCS-type structures, including well-defined bow echoes. The observations are more in agreement with the simulations of Weisman (1993) when the 0–5-km shear is considered, suggesting that the deep-layer shear parameters have more utility in forecasting DCSs. This is supported by the fact that substantial shear is often observed in the 5–10-km layer. Overall, this highlights the need to examine DCS simulations within more realistic environments to help reconcile these disparities in observations and idealized models and to provide improved information to forecasters.

Acknowledgments. The authors greatly appreciate the constructive comments and suggestions provided by two anonymous reviewers. Earlier versions of the manuscript were improved through the very helpful suggestions given by Dr. Lance Bosart, Dr. David Schultz, and Robert Johns. This research was supported in part by a NOAA Career Award and by NSF Grant ATM-0138559 and was made possible under the NOAA-OU Cooperative Agreement NA17RJ1227 for the establishment of CIMMS.

REFERENCES

Atkins, N. T., and R. M. Wakimoto, 1991: Wet microburst activity over the southeastern United States: Implications for forecasting. *Wea. Forecasting,* **6,** 470–482.

Bentley, M. L., and T. L. Mote, 1998: A climatology of derecho-producing mesoscale convective systems in the central and eastern United States, 1986–1995. Part I: Temporal and spatial distribution. *Bull. Amer. Meteor. Soc.,* **79,** 2527–2540.

——, and ——, 2000: Reply. *Bull. Amer. Meteor. Soc.,* **81,** 1054–1057.

——, ——, and S. F. Byrd, 2000: A synoptic climatology of derecho producing mesoscale convective systems in the north-central plains. *Int. J. Climatol.,* **20,** 1329–1349.

Bluestein, H. B., 1993: *Observation and Theory of Weather Systems.* Vol. 2. *Synoptic–Dynamic Meteorology in Mid-Latitudes,* Oxford University Press, 392–407.

Bosart, L. F., W. E. Bracken, A. Seimon, J. W. Cannon, K. D. LaPenta, and J. S. Quinlan, 1998: Large-scale conditions associated with the northwesterly flow intense derecho events of 14–15 July 1995 in the northeastern United States. Preprints, *19th Conf. on Severe Local Storms,* Minneapolis, MN, Amer. Meteor. Soc., 503–506.

Brooks, H. E., C. A. Doswell III, and J. Cooper, 1994: On the environments of tornadic and nontornadic mesocyclones. *Wea. Forecasting,* **9,** 606–618.

Coniglio, M. C., and D. J. Stensrud, 2001: Simulation of a progressive derecho using composite initial conditions. *Mon. Wea. Rev.,* **129,** 1593–1616.

DeGaetano, A. T., 1996: Delineation of mesoscale climate zones in the northeastern United States using a novel approach to cluster analysis. *J. Climate,* **9,** 1765–1782.

Duke, J. W., and J. A. Rogash, 1992: Multiscale review of the development and early evolution of the 9 April 1991 derecho. *Wea. Forecasting,* **7,** 623–635.

Evans, J. S., and S. F. Corfidi, 2000: Genesis and evolution of the 4 June 1999 derecho. Preprints, *21st Conf. on Severe Local Storms,* Orlando, FL, Amer. Meteor. Soc., 405–408.

——, and C. A. Doswell, 2001: Examination of derecho environments using proximity soundings. *Wea. Forecasting,* **16,** 329–342.

Fovell, R. G., and M. Y. Fovell, 1993: Climate zones of the conterminous United States defined using cluster analysis. *J. Climate,* **6,** 2103–2130.

Fujita, T. T., 1978: Manual of downburst identification for Project NIMROD. SMRP Research Paper 156, University of Chicago, 104 pp.

——, and R. M. Wakimoto, 1981: Five scales of airflow associated with a series of downbursts on 16 July 1980. *Mon. Wea. Rev.,* **109,** 1438–1456.

Funk, T. W., K. E. Darmofal, J. D. Kirkpatrick, V. L. DeWald, R. W. Przybylinski, G. K. Schmocker, and Y. J. Lin, 1999: Storm reflectivity and mesocyclone evolution associated with the 15 April

1994 squall line over Kentucky and southern Indiana. *Wea. Forecasting,* **14,** 976–993.
Gale, J. J., W. A. Gallus Jr., and K. A. Jungbluth, 2002: Toward improved prediction of mesoscale convective system dissipation. *Wea. Forecasting,* **17,** 856–872.
Gilmore, M. S., and L. J. Wicker, 1998: The influence of midtropospheric dryness on supercell morphology and evolution. *Mon. Wea. Rev.,* **126,** 943–958.
Goff, R. C., 1976: Vertical structure of thunderstorm outflows. *Mon. Wea. Rev.,* **104,** 1429–1440.
Gong, X., and M. B. Richman, 1995: On the application of cluster analysis to growing season precipitation data in North America east of the Rockies. *J. Climate,* **8,** 897–931.
Hinrichs, G., 1888: Tornadoes and derechos. *Amer. Meteor. J.,* **5,** 306–317, 341–349.
Hookings, G. A., 1965: Precipitation-maintained downdrafts. *J. Appl. Meteor.,* **4,** 190–195.
Houze, R. A., Jr., S. A. Rutledge, M. I. Biggerstaff, and B. F. Smull, 1989: Interpretation of Doppler weather radar displays of midlatitude mesoscale convective systems. *Bull. Amer. Meteor. Soc.,* **70,** 608–619.
Johns, R. H., 1993: Meteorological conditions associated with bow echo development in convective storms. *Wea. Forecasting,* **8,** 294–299.
——, and W. D. Hirt, 1987: Derechos: Widespread convectively induced windstorms. *Wea. Forecasting,* **2,** 32–49.
——, and C. A. Doswell III, 1992: Severe local storms forecasting. *Wea. Forecasting,* **7,** 588–612.
——, and J. S. Evans, 2000: Comments on ''A climatology of derecho-producing mesoscale convective systems in the central and eastern United States, 1986–1995. Part I: Temporal and spatial distribution.'' *Bull. Amer. Meteor. Soc.,* **81,** 1049–1054.
——, K. W. Howard, and R. A. Maddox, 1990: Conditions associated with long-lived derechos—An examination of the large-scale environment. Preprints, *16th Conf. on Severe Local Storms,* Kananaskis Park, AB, Canada, Amer. Meteor. Soc., 408–412.
Johnson, R. H., and P. J. Hamilton, 1988: The relationship of surface pressure features to the precipitation and airflow structure of an intense midlatitude squall line. *Mon. Wea. Rev.,* **116,** 1444–1463.
Kistler, R., and Coauthors, 2001: The NCEP–NCAR 50-year reanalysis: Monthly means CD-ROM and documentation. *Bull. Amer. Meteor. Soc.,* **82,** 247–267.
Klimowski, B. A., R. Przybylinski, G. Schmocker, and M. R. Hjelmfelt, 2000: Observations of the formation and early evolution of bow echoes. Preprints, *20th Conf. on Severe Local Storms,* Orlando, FL, Amer. Meteor. Soc., 44–47.
Maddox, R. A., 1980: Mesoscale convective complexes. *Bull. Amer. Meteor. Soc.,* **61,** 1374–1387.
Martinelli, J. T., R. W. Przybylinski, and Y. J. Lin, 2000: Observational study of a midwestern severe wind mesoscale convective system (MCS) on 29 June 1998: A single Doppler analysis study. Preprints, *20th Conf. on Severe Local Storms,* Orlando, FL, Amer. Meteor. Soc., 382–385.
Miller, D. J., and R. H. Johns, 2000: A detailed look at extreme wind damage in derecho events. Preprints, *20th Conf. on Severe Local Storms,* Orlando, FL, Amer. Meteor. Soc., 52–55.
——, D. L. Andra Jr., and J. S. Evans, 2002: Observations of the 27 May 2001 high-end derecho event in Oklahoma. Preprints, *21st Conf. on Severe Local Storms,* San Antonio, TX, Amer. Meteor. Soc., 13–16.
Moncrieff, M. W., 1992: Organized convective systems: Archetypal dynamical models, mass and momentum flux theory, and parameterization. *Quart. J. Roy. Meteor. Soc.,* **118,** 819–850.
——, and C. Liu, 1999: Convection initiation by density currents: Role of convergence, shear, and dynamical organization. *Mon. Wea. Rev.,* **127,** 2455–2464.
Nolan, R. H., 1959: A radar pattern associated with tornadoes. *Bull. Amer. Meteor. Soc.,* **40,** 277–279.
Parker, M. D., and R. H. Johnson, 2000: Organizational modes of midlatitude mesoscale convective systems. *Mon. Wea. Rev.,* **128,** 3413–3436.
Proctor, F. H., 1989: Numerical simulation of an isolated microburst. Part II: Sensitivity experiments. *J. Atmos. Sci.,* **46,** 2143–2165.
Pryzbylinski, R. W., 1995: The bow echo: Observations, numerical simulations, and severe weather detection methods. *Wea. Forecasting,* **10,** 203–218.
Schmidt, J. M., and W. R. Cotton, 1989: A high plains squall line associated with severe surface winds. *J. Atmos. Sci.,* **46,** 281–302.
Shapiro, A., 1992: A hydrodynamical model of shear flow over semiinfinite barriers with application to density currents. *J. Atmos. Sci.,* **49,** 2293–2305.
Spoden, P. J., C. N. Jones, J. Keysor, and M. Lamm, 1998: Observations of flow structure and mesoscale circulations associated with the 5 May 1996 asymmetric derecho in the lower Ohio valley. Preprints, *19th Conf. on Severe Local Storms,* Minneapolis, MN, Amer. Meteor. Soc., 514–517.
Srivastava, R. C., 1985: A simple model of evaporatively driven downdraft: Application to microburst downdraft. *J. Atmos. Sci.,* **42,** 1004–1023.
Uccellini, L. W., and D. R. Johnson, 1979: The coupling of upper and lower tropospheric jet streaks and implications for the development of severe convective storms. *Mon. Wea. Rev.,* **107,** 682–703.
Wakimoto, R. M., 1982: The life cycle of thunderstorm gust fronts as viewed with Doppler radar and rawinsonde data. *Mon. Wea. Rev.,* **110,** 1060–1082.
——, 2001: Convectively driven high wind events. *Severe Convective Storms, Meteor. Monogr.,* No. 50, Amer. Meteor. Soc., 255–298.
Weisman, M. L., 1993: The genesis of severe, long-lived bow echoes. *J. Atmos. Sci.,* **50,** 645–670.
——, 2001: Bow echoes: A tribute to T. T. Fujita. *Bull. Amer. Meteor. Soc.,* **82,** 97–116.
——, and R. Rotunno, 2002: The role of low-level wind shear in promoting long-lived, severe wind-producing convective systems. Preprints, *21st Conf. on Severe Local Storms,* San Antonio, TX, Amer. Meteor. Soc., 1–4.
Wilks, D. S., 1995: *Statistical Methods in the Atmospheric Sciences.* Academic Press, 467 pp.
Zipser, K. A., 1982: Use of a conceptual model of the life cycle of mesoscale convective systems to improve very-short-range forecasts. *Nowcasting,* K. Browning, Ed., Academic Press, 191–204.